Journal of Electronic Materials (2023) 52:7074–7080
https://doi.org/10.1007/s11664-023-10653-x

TOPICAL COLLECTION: 2022 U.S. WORKSHOP ON PHYSICS AND CHEMISTRY OF II-VI MATERIALS

DLTS Study of Defects in HgCdTe Heterostructure Photodiode

K. Majkowycz[1] · **K. Murawski**[1] · **T. Manyk**[1] · **J. Rutkowski**[1] · **M. Kopytko**[1] · **P. Martyniuk**[1]

Received: 6 December 2022 / Accepted: 28 July 2023 / Published online: 30 August 2023
© The Author(s) 2023

Abstract
Deep-level transient spectroscopy (DLTS) measurements were performed on HgCdTe heterostructure photodiode grown by metal-organic chemical vapor deposition (MOCVD) on GaAs substrate. In order to extract defects from individual layers of the heterostructure, three consecutive etchings were performed. In the first experiment, the $N^+/T/p/T/P^+/n^+$ structure was chemically etched to the N^+ bottom contact to obtain a mesa-type detector. Six localized defects were extracted across the entire photodiode. In the second experiment, the bottom contact was made to the *p*-type absorber. Two localized defects were found in the $p/T/P^+/n^+$ structure. In the third experiment, the top layers were removed and $N^+/T/p$ type detector was made—the cap contact was made to the *p*-type absorber, the bottom to the N^+ layer. Five defect levels were identified, three of which overlap with the first experiment. A deep-trap level located at 183 meV above the top of the valence band was identified within the absorber bandgap. This energy coincides with the activation energy determined from the Arrhenius plot for the dark currents. A defect at the level of ~$0.5E_g$ suggests that the dark current at low reverse bias voltage is dominated by the Shockley–Read–Hall (SRH) mechanism.

Keywords DLTS · deep levels · MOCVD · HgCdTe · SRH mechanism

Introduction

The growth of a high-quality $Hg_{1-x}Cd_xTe$ epitaxial layer for applications in infrared (IR) detectors requires the knowledge and control of many experimental factors causing material defects. Among those influencing the morphology of the layer, one can mention the type of substrate, the orientation of the substrate, the temperature of the substrate during growth, and specific properties resulting from the deposition technique. The high density of internal defects in $Hg_{1-x}Cd_xTe$ epitaxial alloys is considered to be one of the most serious issues in the use of this material for large-format and color infrared matrices.[1,2] There are many structural defects in HgCdTe, including point defects related to metal vacancies, misfit dislocations,[2–4] threading dislocation,[3] stacking faults and twins,[3,5] surface crater defects[6,7] and pyramidal hillocks.[1,8]

✉ K. Majkowycz
kinga.majkowycz@wat.edu.pl

[1] Institute of Applied Physics, Military University of Technology, 2 Kaliskiego St., 00-908 Warsaw, Poland

The presence of defects in semiconductors causes disturbances in their band structure, as a result of which additional levels are created in the band gap and energy bands creating trapping centers for carriers. Their presence reduces the lifetime and mobility of carriers, due to the Shockley–Read–Hall (SRH) generation-recombination mechanism, which determines the usefulness of the material for optoelectronic device fabrication. Deep level transient spectroscopy (DLTS) is one of the methods used to characterize electrically active defects in semiconductors.[9] It is widely used to characterize deep traps in silicon,[10] SiGe alloys,[11] II-VI compounds[12,13] and III-V compounds.[14] It is able to distinguish between majority and minority-carrier traps.[9] It allows us to determine the activation energy of a deep level, its capture cross section, concentration and can distinguish between traps and recombination centers.

DLTS uses a semiconductor structure in which there is a depletion region, typically a Schottky diode and p–n junction. This work, in contrast to the papers showing the results obtained for single junctions,[15,16] presents DLTS results for the HgCdTe heterostructure photodiode grown by metal-organic chemical vapor deposition (MOCVD) on

GaAs substrate. Since the complex heterostructure of the analyzed photodiode contains several depletion regions, the experiment was divided into three stages, described later in the paper.

Measurement Technique

The DLTS signal is obtained from the capacitance transient which originates from the filling and emptying of the defect levels by applying electrical pulses to the sample. Under ideal conditions, the capacitance transient $C(t)$ of the deep level is a simple exponential:[9]

$$\Delta C(t) = \Delta C_0 e^{\frac{-t}{\tau}} \tag{1}$$

with $\Delta C(t) =$ where $C(t) - C_\infty$, C_∞ is the steady state capacitance ($t = \infty$), t is the time and τ is referred to as the time constant. The emission rate is the inverse of the time constant, $e_n = 1/\tau$.

The capacitance of the junction is measured at two points of time, t_1 and t_2, and at different temperatures after applying a voltage pulse V_p. The difference between the times t_1 and t_2 is called the rate window. In the DLTS method used double "box-car" was used to define the rate window.

$$C(t_1) - C(t_2) = \Delta C_0 \left[\exp\left(\frac{-t_1}{\tau}\right) - \exp\left(\frac{-t_2}{\tau}\right) \right] \tag{2}$$

where ΔC_0 is the change in capacitance.

To obtain the energy and apparent cross section, the Arrhenius plot is based on the equation for the emission rate:

$$\ln(T^2/e_n) = \left(\ln \frac{T^2}{\sigma_n v_{\mathrm{th}} \frac{g_0}{g_1} N_c} \right) + \frac{E_A}{kT} \tag{3}$$

where $\frac{g_0}{g_1}$ is degeneracy ratio (g_0—when traps are empty, g_1—when traps are occupied), and E_A is the energy barrier for electron emission, which for defects with non-thermally activated capture cross section and an entropy factor equal to zero could be linked to energy level E_t of defects with: $E_A = E_C - E_t$, k is the Boltzmann constant, T is the absolute temperature, N_c is the density of states in the conduction band, v_{th} is the thermal velocity, and σ is the capture cross section. We used a complete hardware and software system by Semetrol. The sample was mounted in a helium closed-cycle cryostat allowing the temperature to be maintained in the range of 50 to 300 K.

Device Design and Fabrication

The $Hg_{1-x}Cd_xTe$ detector was fabricated with an $N^+/T/p/T/P^+/n^+$ configuration by metal-organic chemical vapor deposition (MOCVD). The HgCdTe epilayer was grown on 2-inch, epi-ready, semi-insulating (100) GaAs substrate after a 3-µm-thick CdTe buffer layer.[17,18] The $N^+/T/p/T/P^+/n^+$ structure consists of four main layers: a heavily In-doped N^+ contact layer with a composition of $x = 0.523$ and a thickness of ~10 µm. Then we have a p-type As-doped absorber with a composition of $x = 0.370$ and a thickness of ~3.3 µm. Next, there is a wide-band gap, heavily As-doped, 2-µm-thick P^+ layer with a composition significantly larger than that of the absorber ($x = 0.536$). The 1-µm-thick n^+ layer with a composition lower than that of the absorber ($x = 0.171$) and donor concentration of about 10^{18} cm^{-3} is on the top of the entire structure. The parameters of the transient T layers are conditioned mainly with the interdiffusion processes during the MOCVD growth.

The detector was designed to be bottom-illuminated through the N^+ layer and optimized for operation at a temperature of 230 K. The cut-off wavelength (λ_c) is conditioned by the Cd composition of the active layer and operating temperature. At 230 K, λ_c determined at 50% of the maximal signal is about 3.25 µm (see Fig. 1).

Figure 2 shows the current density–voltage (J–V) and capacitance–voltage (C–V) characteristics of the $N^+/T/p/T/P^+/n^+$ photodiode. A strongly asymmetric nature of the J–V curves was observed, indicating excellent rectifying behaviors, which means that the current flows through the p–n junction in one direction only. C–V measurements were also performed to define the

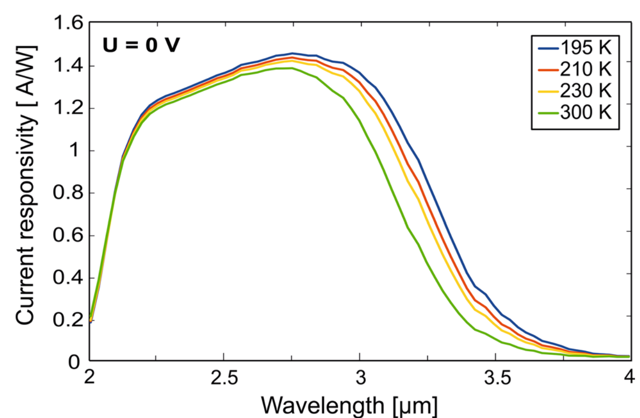

Fig. 1 Current responsivity for backside illuminated HgCdTe $N^+/T/p/T/P^+/n^+$ photodiode operating at selected temperatures.

depletion width of the diode. The value of the junction capacitance at zero bias is of the order of 30 pF, which proves that the measurement can be made using the DLTS method.

Experiment

DLTS studies were carried out on mesas with an area of 400 μm × 400 μm. Detector mesas were defined by standard optical photolithography and wet chemical etching with Br:HBr (1:100) diluted in deionized water (50:50:1 Br:HBr:H_2O) solution. Cr/Au contacts were deposited on the top and bottom contact layers.

In order to extract defects from individual layers of the heterostructure, three consecutive etchings were performed for the same epitaxial layer. In the first experiment, the etching was performed through the entire N^+/T/p/T/P^+/n^+ structure to the N^+ bottom contact (Fig. 3a). In the second experiment, the bottom contact was made to the *p*-type absorber—p/T/P^+/n^+ structure (Fig. 3b). In the third experiment, the top layers were removed and a N^+/T/p type detector was made—the cap contact was made to the *p*-type absorber and the bottom to the N^+ layer (Fig. 3c).

Results

Figure 4 shows calculated band profiles for the analyzed photodiode operating at zero and 0.2 V reverse bias voltage, and the temperature of 230 K. Calculations were made by commercially available APSYS software. The calculated band diagram for the N^+/T/p/T/P^+/n^+ HgCdTe heterostructure shows three junctions (see Fig. 4a). The highest voltage is deposited at the junction between the absorber and bottom contact layer and extends deep into the absorber layer. It follows that the DLTS method can be used for such a structure, because the measured transient capacitance can only be attributed to changes in the junction capacitance associated with the HgCdTe absorber. To confirm this, the

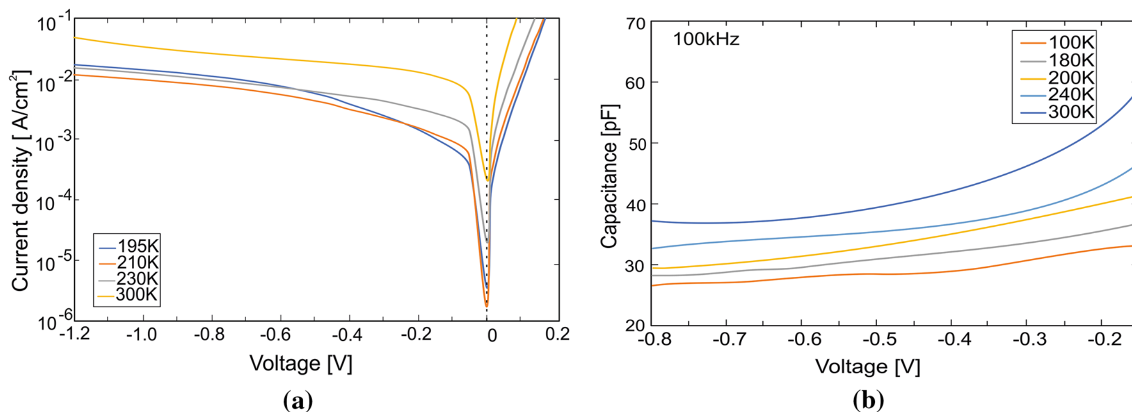

Fig. 2 Current–voltage characteristics (a) and capacitance–voltage characteristics (b) for HgCdTe N^+/T/p/T/P^+/n^+ photodiode operating at selected temperatures.

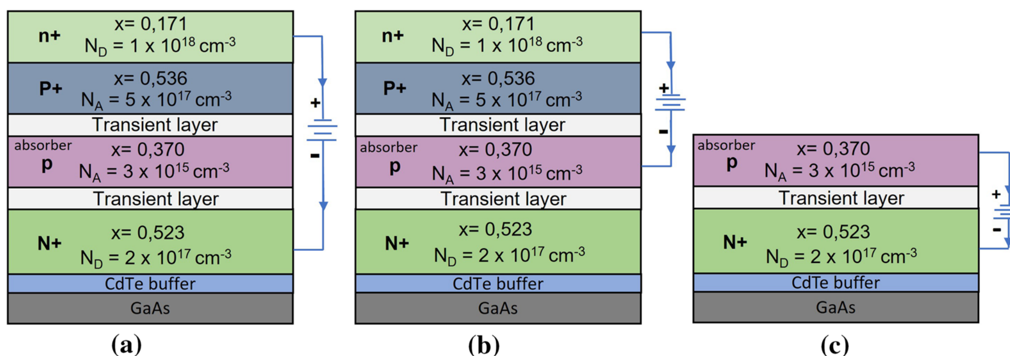

Fig. 3 Three chemical etching procedures for DLTS measurement: (a) the N^+/T/p/T/P^+/n^+ structure was chemically etched to the N^+ bottom contact; (b) the bottom contact was made to the absorber—p/T/P^+/n^+ structure; (c) electrical contact between *p*-type absorber and N^+ layer—N^+/T/p structure.

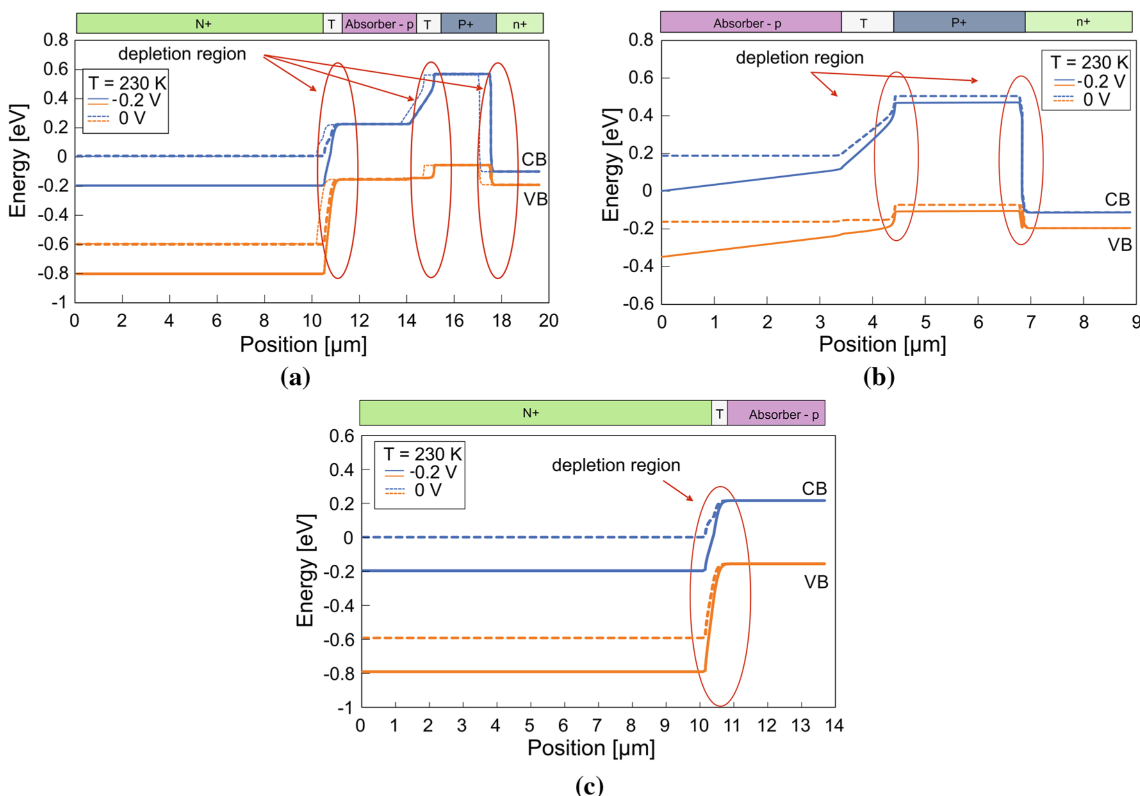

Fig. 4 Calculated band diagrams for HgCdTe heterostructure detector $N^+/T/p/T/P^+/n^+$ (a) and division of the heterostructure into single p-n junctions (b) $p/T/P^+/n^+$ structure; (c) $N^+/T/p$ structure. The orange line is the valence band (VB) and the blue line is the conduction band (CB). Calculations were made at a temperature of 230 K (Color figure online).

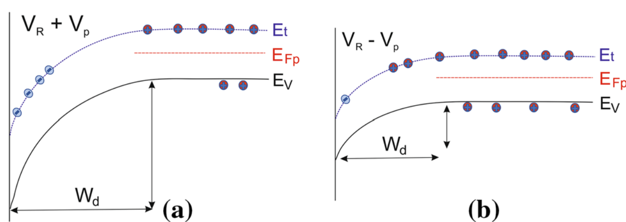

Fig. 5 Scheme of filling the traps in the *p*-type absorber at (a) negative fill pulse, (b) positive fill pulse.

experiment was divided into three parts (see Fig. 4b and c). In the second experiment, two junctions are visible: p–P^+ and P^+–n^+, which are not present in the third experiment. The third experiment contains only one junction (N^+–p), which is the dominant junction for the entire photodiode.

DLTS measurements were performed for two frequencies, 100 kHz and 300 kHz, with the rate window (RW) values of 144 s^{-1} and 240 s^{-1} respectively, and filling pulse width t_p = 1 ms. In the first experiment, the voltage applied to the device during the measurement (bias voltage) was set to $V_R = -1.2$ V and the voltage applied to fill traps (fill pulse) was set to $V_p = -0.4$ V and $V_p = 0.4$ V. In two successive experiments, the bias voltage was set to $V_R = -1$ V and the fill pulse was set to $V_p = -0.2$ V and $V_p = 0.2$ V. The applied reverse bias voltage has determined the width of the space charge region in the *p*-type absorber. The negative fill pulse caused the trap levels to be filled with electrons in the space charge region (see Fig. 5a). After the negative pulse ceased, the reverse voltage was restored and electrons were emitted into the conduction band (CB). The applied positive fill pulse filled the trap levels with holes (see Fig. 5b), and after the cessation of the pulse, holes were emitted into the valence band (VB).

DLTS spectra performed for three experiments is shown in Fig. 6. Six localized defects were found across the entire $N^+/T/p/T/P^+/n^+$ photodiode (first experiment shown in Fig. 6a). DLTS using 300-kHz capacitance measurements revealed one trap with a positive fill pulse (peak B) and four traps with a negative fill pulse (peaks A, D, E, F). DLTS spectra using 100-MHz capacitance measurements were also taken and compared with those at 300 kHz. One trap was revealed at a frequency of 100 kHz (peak C) which does not overlap with the measurement at 300 kHz. Since for the entire $N^+/T/p/T/P^+/n^+$ photodiode it is difficult to clearly determine which of these traps are localized in the absorber and whether they are electron traps or hole traps, DLTS measurement was performed for the isolated junctions. Two localized defects were found in the second experiment

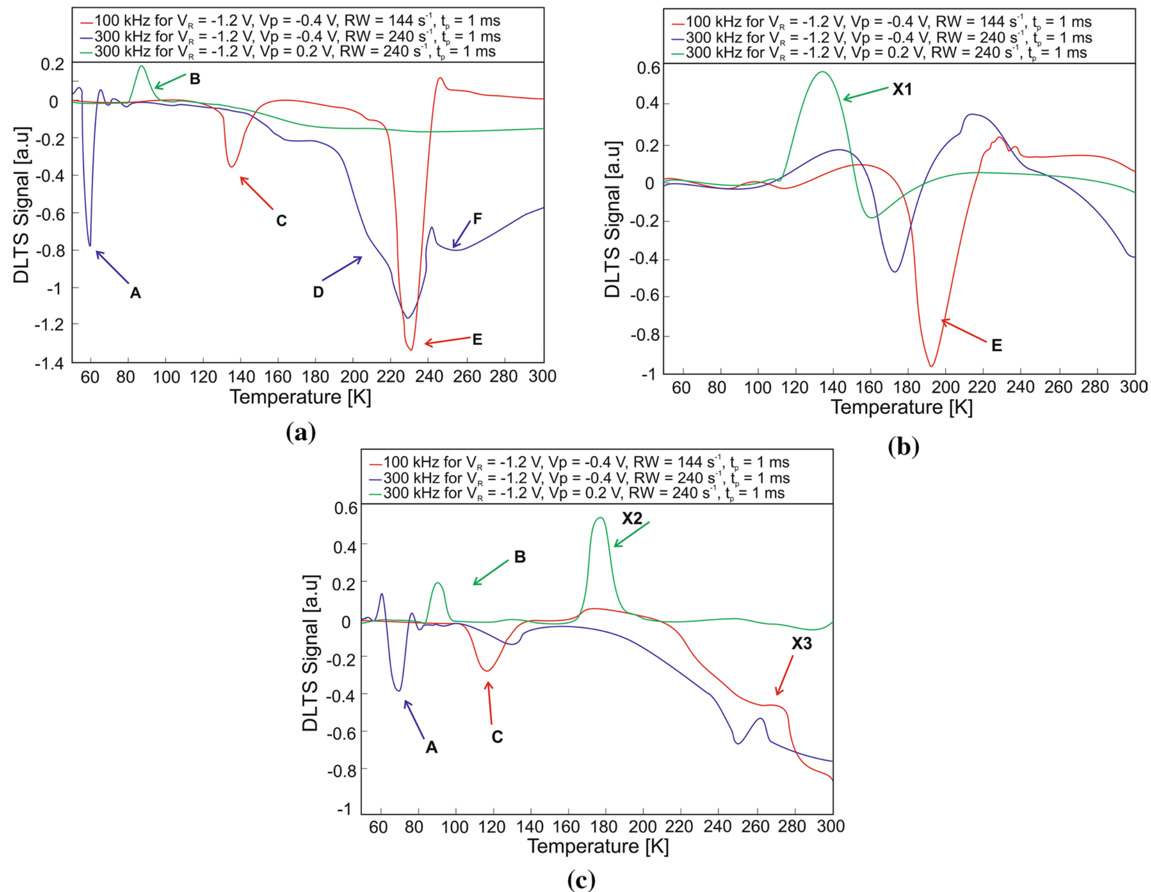

Fig. 6 DLTS signal for first ($N^+/T/p/T/P^+/n^+$ structure) (a), second ($p/T/P^+/n^+$ structure) (b) and third ($N^+/T/p$ structure) experiment (c). The red and blue lines were designated at negative V_p, and the green line was designated at positive V_p (Color figure online).

performed for the $p/T/P^+/n^+$ structure (Fig. 6b). One trap (peak E) overlaps with the first experiment and is not present in the third one ($N^+/T/p$ structure). This suggests that it most likely comes from one of the upper layers etched off for the third experiment. Five defect levels were identified in the third experiment—$N^+/T/p$ structure (Fig. 6c), and three of them (peaks A, B, and C) overlap with the first experiment. The traps associated with these peaks can be considered to lie in the absorber layer. A and C are assigned to the electron traps (revealed with a negative fill pulse) while B is assigned to the hole trap (revealed with a positive fill pulse).

Moreover, the shape of the A, B, C, and E DLTS peaks suggests point defects, probably related to mercury vacancies or impurity atoms which occupy anion or cation sites.[17,18] DLTS peaks from point defects are narrow and symmetrical, and their extremes do not change position with increasing time needed to fill traps, while for extended defects the DLTS signal line is always widened and the position of the signal maximum remains almost constant when changing the length of the filling pulse.

Arrhenius plots for the entire and divided structure are presented in Fig. 7. DLTS parameters such as capture cross sections for carriers and activation energies are shown in Table I. Three activation energies for peaks A, B, and C obtained from the first experiment overlap with the activation energies from the third experiment. Activation energies indicate that these defects are located within the absorber's bandgap ($E_g = 354$ meV at 77 K and $E_g = 385$ meV at 300 K). B is estimated to have an energy level at $E_V + 183$ meV and a hole-capture cross section of 4.1×10^{-12} cm^2. A (C) has a level at $E_C - 283$ meV ($E_C - 267$ meV), an electron capture cross section of 5×10^{-16} cm^2 (2.6×10^{-15} cm^2), averaged over two experiments. The classical trap is characterized by a large capture cross section in the range of 10^{-15}–10^{-12} cm^2, then the cascading process is dominant.[19] The others traps, with capture cross sections in the range of 10^{-16}–10^{-15} cm^2, are neutral.[20]

As mentioned earlier, the E peak comes from one of the upper layers. Considering the activation energy equal to 479 meV, it is most likely located within the bandgap of the wide-gap P^+ layer ($E_g = 625$ meV at 77 K and $E_g = 616$ meV at 300 K). Activation energy equal to 618 meV for the F peak, which is visible only in the first

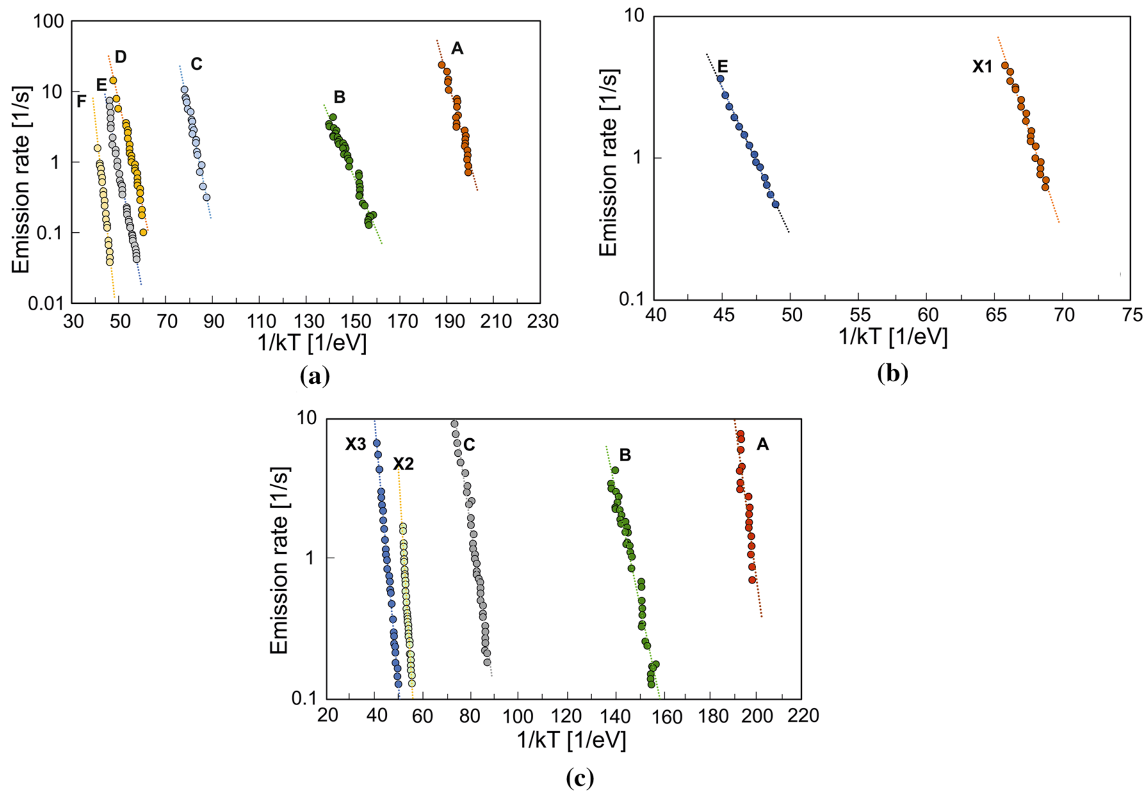

Fig. 7 Arrhenius plot of emission rate for first (N^+/T/p/T/P^+/n^+ structure) (a), second (p/T/P^+/n^+ structure) (b) and third (N^+/T/p structure) experiment (c).

Table I The trap energies and capture cross sections found by the DLTS method

Peak	Experiment I		Experiment II		Experiment III	
	E_a (meV)	σ (cm^2)	E_a (meV)	σ (cm^2)	E_a (meV)	σ (cm^2)
A	283	5.0×10^{-13}			283	4.8×10^{-13}
B	183	4.1×10^{-12}			183	4.1×10^{-12}
C	261	1.2×10^{-16}			274	5.2×10^{-15}
D	338	4.1×10^{-16}				
E	400	2.2×10^{-16}	476	6.4×10^{-15}		
F	618	2.4×10^{-16}				
X1			677	1.5×10^{-8}		
X2					621	1.8×10^{-10}
X3					432	5.5×10^{-15}

experiment, is close to the bandgap of the P^+ layer and is much larger than the energy gap for other photodiode layers. Activation energies higher than the energy gap can be explained by two effects. First, the activation energy is not an energy level in the band structure but an enthalpy change. Second, the cross section of the capture can also be thermally activated.

Figure 8 shows the Arrhenius plot of the dark current measured at 0.1 V reverse biased N^+/T/p/T/P^+/n^+ photodiode. The estimated thermal activation energy of ~183 meV is close to $0.5E_g$, what suggests that the dark current at low reverse bias is dominated by the SRH mechanism. This activation energy coincides with the DLTS trap located at the energy level of $E_V + 183$ meV.

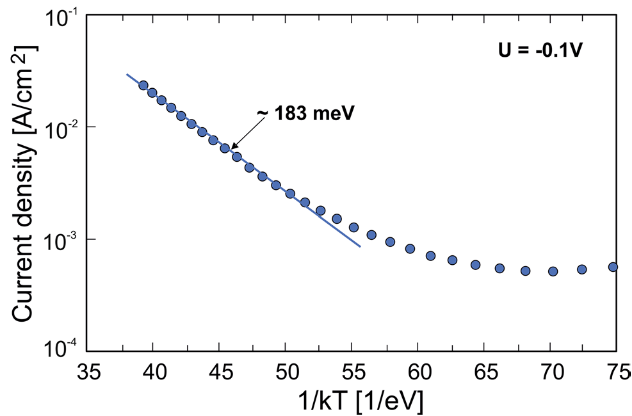

Fig. 8 Current density as a function of 1/kT for U = −0.1 V and activation energy obtained from the slope of the curve.

Conclusions

The paper presents the possibilities of DLTS analysis of a complex heterostructure containing several depletion regions. Performing three different experiments separating individual junctions of the heterostructure allows determining which layer the trap comes from. Three peaks A, B, and C with activation energies of $E_C - 283$ meV, $E_V + 183$ meV, and $E_C - 267$ meV were detected within the absorber band gap. The deep trap level located at the energy of 183 meV above the top of the valence band coincides with the activation energy determined from the Arrhenius plot for the dark current. The activation energy corresponds to ~$0.5E_g$, which means that the dark current at low reverse bias is dominated by the SRH mechanism. The determined electron capture cross section for this trap is 4.1×10^{-12} cm^2. The E peak with the activation energy of 479 meV is most likely located within the bandgap of the wide-gap P$^+$ layer.

Funding This study was funded by the National Science Centre (Poland), Grant No. UMO-2019/33/B/ST7/00614.

Conflict of interest The authors declare that they have no conflict of interest.

Open Access This article is licensed under a Creative Commons Attribution 4.0 International License, which permits use, sharing, adaptation, distribution and reproduction in any medium or format, as long as you give appropriate credit to the original author(s) and the source, provide a link to the Creative Commons licence, and indicate if changes were made. The images or other third party material in this article are included in the article's Creative Commons licence, unless indicated otherwise in a credit line to the material. If material is not included in the article's Creative Commons licence and your intended use is not permitted by statutory regulation or exceeds the permitted use, you will need to obtain permission directly from the copyright holder. To view a copy of this licence, visit http://creativecommons.org/licenses/by/4.0/.

References

1. A. Rogalski and Z. Bielecki, *Detection of Optical Signals* (Boca Raton: CRC Press, 2022).
2. A. Szilagyi and M.N. Grimbergen, Misfit and threading dislocations in HgCdTe epitaxy. *JVSTA* 4, 2200 (1986).
3. Y. Chang, C.R. Becker, C.H. Grein, J. Zhao, C. Fulk, T. Casselman, R. Kiran, X.J. Wang, E. Robinson, S.Y. An, S. Mallick, S. Sivananthan, T. Aoki, C.Z. Wang, D.J. Smith, S. Velicu, J. Zhao, J. Crocco, Y. Chen, G. Brill, P.S. Wijewarnasuriya, N. Dhar, R. Sporken, and V. Nathan, Surface morphology and defect formation mechanisms for HgCdTe (211)B grown by molecular beam epitaxy. *J. Electron. Mater.* 5, 5000 (2008).
4. B. Yang, Y. Xin, and S. Rujirawat, Molecular beam epitaxial growth and structural properties of HgCdTe layers on substrates. *J. Appl. Phys.* 88, 115 (2000).
5. N. Oda, T. Kanno, M. Saga, R. Oikawa, and Y. Maejima, Composition characterization methods for HgCdTe epilayers grown by molecular beam epitaxy. *J. Cryst. Growth* 117, 193 (1992).
6. C.J.S.L.H. Zhang, A study of void defects in metalorganic molecular-beamepitaxy grown HgCdTe. *J. Electron. Mater.* 27, 634 (1998).
7. L. He, X. Fu, Q. Wei, W. Wang, L. Chen, Y. Wu, X. Hu, J. Yang, Q. Zhang, R. Ding, X. Chen, and W. Lu, MBE HgCdTe on alternative substrates for FPA applications. *J. Electron. Mater.* 37, 1189 (2008).
8. R.J. Koestner and H.F. Schaake, Kinetics of molecular-beam epitaxial HgCdTe growth. *JVSTA* 6, 2834 (1988).
9. D.V. Lang, Deep-level transient spectroscopy: a new method to characterize traps in semiconductors. *J. Appl. Phys.* 45, 3023 (1974).
10. S.D. Brotherton and P. Bradley, Defect production and lifetime control in electron and γ-irradiated silicon. *J. Appl. Phys.* 53, 5720 (1982).
11. L. Dobaczewski, K. Gościński, K. Bonde Nielsen, A. Nylandsted Larsen, J. Lundsgaard Hansen, and A.R. Peaker, Alloy splitting of gold and platinum acceptor levels in SiGe. *Phys. Rev. Lett.* 83, 4582 (1999).
12. D.L. Polla and C.E. Jones, Deep level studies of $Hg_{1-x}Cd_xTe$. I: narrow-band-gap space-charge spectroscopy. *J. Appl. Phys.* 52, 5118 (1981).
13. D.L. Polla, S.P. Tobin, and M.B. Reine, Experimental determination of minority-carrier lifetime and recombination mechanisms in p-type $Hg_{1-x}Cd_xTe$. *J. Appl. Phys.* 52, 5182 (1981).
14. F.D. Auret and M. Nel, Deep level transient spectroscopy of hole defects in bulk-grown p-GaAs using Schottky barrier diodes. *Appl. Phys. Lett.* 48, 130 (1986).
15. L. Rubaldo, A. Brunner, J. Berthoz, N. Pere-Laperne, A. Kerlain, P. Abraham, D. Bauza, G. Reimbold, and O. Gravrand, Defects study in $Hg_xCd_{1-x}Te$ infrared photodetectors by deep level transient spectroscopy. *J. Electron. Mater.* 43, 3065 (2014).
16. P. Guinedor, T. Broult, A. Brunner, L. Rubaldo, D. Bauza, G. Reimbold, A. Kerlain, and V. Destefanis, DLTS study of extended defects in HgCdTe photodiodes. *J. Phys.* 1190, 120 (2018).
17. A. Kobayashi, O.F. Sankey, and J.D. Dow, Chemical trends for defect energy levels in $Hg_{(1-x)}Cd_xTe$. *Phys. Rev. B* 25, 6367 (1982).
18. C.W. Myles, Charge state splittings of deep levels in $Hg_{1-x}Cd_xTe$. *JVSTA* 6(4), 2675 (1988).
19. M. Lax, Cascade capture of electrons in solids. *Phys. Rev.* 119, 1502 (1960).
20. P. Blood and J.W. Orton, *The Electrical Characterization of Semiconductors: Majority Carriers and Electron States* (New York: Academic Press, 1992).

Publisher's Note Springer Nature remains neutral with regard to jurisdictional claims in published maps and institutional affiliations.